Percolation and transport coefficients of biaxial anisotropic composites

1992 J. Phys.: Condens. Matter 4 1521

(http://iopscience.iop.org/0953-8984/4/6/017)

J. Phys.: Condens. Matter 4 (1992) 1521–1533. Printed in the UK

Percolation and transport coefficients of biaxial anisotropic composites

Asya Skal† and Igor Grebnev‡
A F Ioffe Physico-Technical Institute, Academy of Science of the USSR, 194021 Leningrad, USSR

Received 25 June 1990, in final form 3 August 1991

Abstract. Second-order phase transitions are studied for a biaxial anisotropic disordered system composed of randomly distributed metal and non-metal regions, the former having tensor-type conductivity along the principal axes. Integrals are derived for the anisotropic Hall and Seebeck coefficients using Green functions. Computer calculations show that near the percolation threshold, the decrease of the biaxial anisotropy of the effective conductivity and Hall and Seebeck coefficients is described by new critical exponents. A model of 'special points' of the biaxial anisotropic infinite cluster above the threshold and the two-component infinite cluster below the threshold is developed.

1. Introduction

This paper is a sequel to and a further development of Skal (1981a, b, 1982a, 1985, 1987) and Skal *et al* (1982) dealing with percolation in isotropic and anisotropic media.

Natural uniaxial anisotropy is demonstrated, for example, by a layered crystal similar to graphite, or by quasi-one-dimensional crystals of the tetracyanoquinodimethane (TCNQ) type. If there is a strong magnetic field along another axis, these crystals become biaxial anisotropic ones.

Let us start with a simple biaxial model of anisotropy and find out what new exponents result from it. A random two-component mixture has a geometrically isotropic distribution of components, one of which is characterized by the tensor

$$\hat{\sigma}_1 = \begin{pmatrix} \sigma_x & 0 & 0 \\ 0 & \sigma_y & 0 \\ 0 & 0 & \sigma_z \end{pmatrix} \qquad a = \sigma_x/\sigma_z \qquad b = \sigma_y/\sigma_z \tag{1}$$

and the other by the scalar σ_2, where a and b are the anisotropic parameters.

† Present address: Physics Department, Ariel College of Judea and Samaria, Ariel, Efraim 44820, Israel.
‡ Present address: Applied Physics Department, Hebrew University, Givat Ram, Jerusalem 91904, Israel.

0953-8984/92/061521 + 13 $04.50

Uniaxial anisotropic percolation was first studied by Shklovskii (1978) who used the SSDG (Skal and Shklovskii 1974, De Gennes 1976) idealized superlattice model, with the nodes connected by one-dimensional links, and introduced the critical exponent λ:

$$A(a,p) = \frac{\sigma_x^{\text{eff}}(a,p)}{\sigma_y^{\text{eff}}(a,p)} = 1 + \text{const}(p - p_c)^{\lambda} \qquad \lambda = \xi - \nu, \lambda = 0.3 \tag{2}$$

where $\sigma_x^{\text{eff}}(p)$ and $\sigma_y^{\text{eff}}(p)$ are the effective conductivities along the respective coordinate axes, ν is the exponent of the infinite cluster correlation radius, which is equal to the distance between the superlattice nodes, and ξ is the exponent of the one-dimensional links that connect the superlattice nodes along the cluster. With the de Gennes postulated value $\xi = 1$ for all dimensionalities, and with universally accepted $\nu_2 = 1.3$ and $\nu_3 = 0.8$ one can obtain $\lambda_2 < 0$ and $\lambda_3 = 0.2$ (here and below we use the subscripts according to the dimensionality of the space). However, $\lambda_2 < 0$ is not true because the anisotropic effect decays at a faster rate than the conductivity: Vannimenus and Knezevic (1984) obtained $\nu_2/\lambda_2 = 0.306$ and $\nu_3/\lambda_3 = 0.3$; Sarychev and Vinogradov (1983) found $\lambda_2 = 0.9$ and $\lambda_3 = 0.3$; Straley (1980) calculated $\lambda = 1$ for the Cayley tree and $\lambda = 3$ for a high-dimensional limit; and Lobb *et al* (1981) found $\nu_2/\lambda_2 = 0.67$.

If a tends to 1, then the left part of formulae (2) also tends to 1 but the second term in the right part of (2) does not disappear and so it cannot be used for all values of a. Skal (1987) suggested the existence of two universal curves that characterize the transition to the quasi-one-dimensional $f_1(p)$ and the quasi-two-dimensional $f_2(p)$ states, each with a critical exponent of its own:

$$A(a,p) = \begin{cases} f_1(p) = 1 + \text{const}(p - p_c)^{\lambda_{31}} & a \to \infty \\ f_2(p) = 1 + \text{const}(p - p_c)^{\lambda_{32}} & a \to 0 \end{cases} \tag{3}$$

where $\lambda_{31} = 0.45 \pm 0.05$ and $\lambda_{32} = 0.15 \pm 0.05$ are the quasi-exponents of the quasi-one- and two-dimensional transitions, respectively. The number of exponents increases with dimensionality; for example, in two-dimensional systems there is only one exponent λ_2. Comparision of this result with other authors' findings presents difficulties because the data in the literature refer only to a single exponent in two and three dimensions.

2. Calculation of the anisotropic Hall coefficient

The formula for the Hall coefficient in an isotropic disordered system was obtained by Skal (1981a, 1985) using the reciprocity theorem. In this paper a new strict method for calculating the anisotropic Hall coefficient using the Green function is proposed. After deriving the formula for the anisotropic Hall coefficient in the continuum we will pass to a two-component medium. Let us consider a disordered system whose discontinuity scale is larger than the free path of charge carriers and the cyclotron radius, the radius, in turn, being smaller than the free path. Such a medium permits the introduction of the local conductivity tensor (1) and the Hall coefficient $R(r)$. Let the sample be a cube with the side length $L_{x_1}, L_{x_2}, L_{x_3}$, where $x = x_1$, $y = x_2$ and $z = x_3$. We apply the electric field with potential $-\varphi_m(r)$ where $m = 1, 2, 3$. We will consider weak magnetic fields and solve the problem of calculating the effective Hall coefficient in first order on the applied magnetic field. If the electric field is directed along the axis m and the magnetic

field along the axis k, the equation for the projection of the total current on the axis n in the tensor form is written as

$$j_n^m(r) = \sigma_{nk}(r)\nabla_k\varphi_m(r) + \varepsilon_{skl}\sigma_{ns}(r)H_k\sigma_{lt}(r)\nabla_t\varphi_m(r)R(r) \tag{4}$$

where ε_{skl} is an antisymmetric tensor, the recurrent subscripts are summed, the boundary conditions on the potential are $\varphi_m(r)|_{r\in\Gamma} = Ex_m$, and Γ is the boundary surface of the sample.

Let us expand the solution into a series in the quadratic field term

$$j(r) = j_0(r) + j_1(r) + O(H^2) \qquad \varphi_m(r) = \varphi_{0,m}(r) + \varphi_{1,m}(r) + O(H^2) \tag{5}$$

$$\begin{aligned} j_{0,n}^m(r) &= \sigma_{nk}(r)\nabla_k\varphi_{0,m}(r) \\ j_{1,n}^m(r) &= \sigma_{nk}(r)\nabla_k\varphi_{1,m}(r) + \lambda_{nl}(r)\nabla_t\varphi_{0,m}(r) \end{aligned} \tag{6}$$

where we introduce

$$\lambda_{nl}(r) = \varepsilon_{skl}\sigma_{ns}(r)H_k\sigma_{lt}(r)R(r).$$

The boundary conditions for the potentials in the first and zeroes approximations are

$$\varphi_{0,m}(r)|_{r\in\Gamma} = Ex_m \qquad \varphi_{1,m}(r)|_{r\in\Gamma} = 0.$$

Using the equations $\nabla j_0(r) = 0$ and $\nabla j_1(r) = 0$ the system (6) can be rewritten in the form

$$\begin{aligned} &\nabla_n[\sigma_{nk}(r)\nabla_k\varphi_{0,m}(r)] = 0 \\ &\nabla_n[\sigma_{nk}(r)\nabla_k\varphi_{1,m}(r)] = -\nabla_n[\lambda_{nl}(r)\nabla_t\varphi_{0,m}(r)]. \end{aligned} \tag{7}$$

Here we introduce a new function $\varphi'_{0,m}(r) - Ex_m$ which has zero boundary conditions but is characterized by a more complex equation

$$\nabla_n[\sigma_{nk}(r)\nabla_k\varphi'_{0,m}(r)] = -\nabla_n[\sigma_{nk}(r)\nabla_k Ex_m] \tag{8}$$

and permits a Green function $G(r, r)$ solution

$$\nabla_n[\sigma_{nk}(r)\nabla_k G(r, r')] = \delta(r - r') \qquad G(r, r')|_{r\in\Gamma} = 0 \qquad G(r, r') = G(r', r)$$

$$\begin{aligned} \varphi'_{0,m}(r) &= -\int_{V'} G(r, r')\nabla'_n[\sigma_{nk}(r')\nabla'_k Ex'_m]\,dV' \\ &= E\int_{V'} \sigma_{nk}(r')\delta_k^m\nabla'_n G(r, r')\,dV'. \end{aligned} \tag{9}$$

here $\nabla'_k x'_m = \delta_k^m$, δ_k^m is the Kronecker delta.

The last integral is obtained through integration by parts taking into account zero boundary conditions for the Green function. The transition to the potential in zeroth approximation yields the equation

$$\varphi_{0,m}(r) = Ex_m + E\int_{V'} \sigma_{nm}(r')\nabla'_n G(r, r')\,dV' \tag{10}$$

and makes it possible to calculate the current density in the zeroth approximation (6):

$$j_{0,n}^m(r) = \sigma_{nk}(r)E\delta_k^m + E\int_{V'} \sigma_{nk}(r)\sigma_{lm}(r')\nabla_k\nabla'_l G(r, r')\,dV'. \tag{11}$$

This equation permits computation of the integral of the Green function and is thus of

primary importance for both the Hall current and the thermal current, which will be similarly obtained below, and therefore we shall rewrite it in a more convenient form, viz.

$$\int_{V'} \sigma_{nk}(r)\sigma_{tm}(r')\nabla_k\nabla'_t G(r,r')\,\mathrm{d}V' = E^{-1}j^m_{0,n}(r) - \sigma_{nm}(r). \tag{12}$$

Now we must do the first approximation calculations of the potential

$$\varphi_{1,m}(r) = -\int_{V'} G(r,r')\nabla'_k[\lambda_{kt}(r')\nabla'_t\varphi_{0,m}(r')]\,\mathrm{d}V$$

$$= \int_{V'} \lambda_{kt}(r')\nabla'_t\varphi_{0,m}(r')\nabla'_k G(r,r')\,\mathrm{d}V \tag{13}$$

to be further used to express the mean Hall current

$$\langle j^m_{1,n}\rangle = \langle\lambda_{nl}\nabla_l\varphi_{0,m}\rangle + \int_V \lambda_{kt}(r')\nabla'_t\,\varphi_{0,m}(r')\sigma^{-1}(r')$$

$$\times \int_V \sigma_{ps}(r')\sigma_{nl}(r)\nabla_l\nabla'_s G(r,r')\,\mathrm{d}V\,\mathrm{d}V' \tag{14}$$

where we define

$$\langle j^m_{1,n}\rangle = \int_V j^m_{1,n}(r)\,\mathrm{d}V.$$

The inner integral is to be taken from equation (12); as a result one can obtain

$$\langle j^m_{1,n}\rangle = \langle\lambda_{nl}\nabla_l\varphi_{0,m}\rangle + \int_V \lambda_{kl}(r)\nabla_l\varphi_{0,m}(r)\sigma^{-1}_{pk}(r)E^{-1}j^n_{0,p}(r)\,\mathrm{d}V$$

$$- \int_V \lambda_{kl}(r)\nabla_l\varphi_{0,m}(r)\sigma^{-1}_{pk}(r)\sigma_{ph}(r)\,\mathrm{d}V. \tag{15}$$

The first and third components are equal, so they are cancelled. Now substitute the value of $\lambda(r)$ from the definition to obtain

$$\langle j^m_{1,n}\rangle = E^{-1}\int_V \varepsilon_{sql}\sigma_{ks}(r)H_q\sigma_{lt}(r)R(r)\nabla_t\varphi_{0,m}(r)\varphi^{-1}_{pk}(r)j^n_{0,p}(r)\,\mathrm{d}V$$

$$= E^{-1}\int_V \varepsilon_{sql}H_q j^m_{0,l}(r)j^n_{0,s}(r)R(r)\,\mathrm{d}V. \tag{16}$$

The effective Hall coefficient is very easily expressed so in the case of applying electric field along axis 'x' and measuring Hall coefficient along 'y' we obtain a formula in a scalar vector form:

$$R^{\mathrm{eff}}(p) = \int_V (j^x_0(r)\cdot[H\times j^y_0(r)])R(r)\,\mathrm{d}V/\sigma^{\mathrm{eff}}_x(p)\sigma^{\mathrm{eff}}_y(p)E^2HV. \tag{17}$$

Thus the problem is reduced to the zeroth approximation calculation of two currents which can be found from a set of Kirchhoff equations by applying the electric field along the 'x' and 'y' axes.

The same procedure is applicable for deriving the equation for the magnetic resistance, which it is possible to find for the isotropic case:

$$\Delta\rho_{mn}(p) = \int_V (j_0^m(r) \cdot [\boldsymbol{H} \times j_1^n(r)])R(r)\,\mathrm{d}V/U_0^2\sigma_n^{\mathrm{eff}}(p)\sigma_m^{\mathrm{eff}}(p). \tag{18}$$

Here the $\sigma_n^{\mathrm{eff}}(p)$ and $\sigma_m^{\mathrm{eff}}(p)$ are the effective conductivities along the n and m axes, and U_0 is the potential difference.

It is only the first component that makes this equation difficult to apply, because percolation theory provides no algorithms for the calculation of the currents $j_1(r)$. However, if the iteration method is used by setting in each node a local Hall EMF equal to the product of the ohmic current density $j_0(r)$ and the Hall coefficient of this node, then the problem can be simplified considerably through use of the model of an infinite cluster with special points (Skal 1987). The model will be reported in detail below (see section 7); the 'active points' of the EMF are found at the maxima of the integrand in (17) and held responsible for those Hall currents that pierce the sample and generate the outside Hall current; the feature of the 'hot points' of the conductivity is that nearly all the Joule heat is released there. These two types of 'special points' affect the Hall effect in different ways: the former are responsible for the effective EMF, while the latter are in charge of the cyclic Hall currents inside the sample because they are associated with heavier ohmic current flows and larger local Hall EMF values. The total Hall current can be found only through use of a model with 'special points' The number of these points over the critical interval is small, so that at the threshold there remains a single point of finite volume, which reduces the number of iterations substantially.

The matter of primary importance for phase transitions is the appearance of new 'special points' described by the index law. Equation (18) makes it clear that the points where the integrals of the first and third components take maximum values are 'special' magnetic points, and by assigning Hall EMF values to these points we can calculate the current density in a second approximation.

3. Calculation of the anisotropic Seebeck coefficient

Let us assume that the medium can be described by thermal conductivity tensor $\hat{\kappa}(r)$ of the form (1) and by the tensor Seebeck coefficient $\hat{\alpha}(r)$, and use the Green function method again. Let us write the system of equations for projections of the current density and the thermal flux $u(r)$ onto the axis along which the electric field is directed:

$$\begin{aligned} j_m(r) &= \sigma_{mk}(r)\nabla_k\varphi(r) - \sigma_{mk}(r)\alpha_{kl}(r)\nabla_l T(r) \\ u_m(r) &= -\kappa_{mk}(r)\nabla_k T(r) + \alpha_{mk}(r)\sigma_{kl}(r)\,T(r)\nabla_l\varphi(r). \end{aligned} \tag{19}$$

The boundary conditions on the potential are established by the fact that opposite edges of the sample are connected and their temperatures are T_1 and T_2.

Using the equalities $\nabla j(r) = 0$ and $\nabla u(r) = 0$ we can rewrite the system in the form

$$\begin{aligned} \nabla_m[\sigma_{mk}(r)\nabla_k\varphi(r) - \sigma_{mk}(r)\alpha_{kl}(r)\nabla_l T(r)] &= 0 \\ \nabla_m[-\kappa_{mk}(r)\nabla_k T(r) + \alpha_{mk}(r)\sigma_{kl}(r)T(r)\nabla_l\varphi(r)] &= 0. \end{aligned} \tag{20}$$

In order to show that in first order in terms of $\alpha(r)$ the second term in the first equation

can be neglected, which helps us calculate the temperature $T_0(r)$ from the set of Kirchhoff equations, we will rewrite the system in the first and zeroth approximation as

$$\nabla[-\hat{\kappa}(r)\nabla T_0(r)] = 0$$
$$\nabla[\hat{\sigma}(r)\nabla\varphi_0(r)] = 0 \tag{21}$$

$$\nabla[\hat{\sigma}(r)\nabla\varphi_1(r)] = \nabla[\hat{\sigma}(r)\hat{\alpha}(r)\nabla T_0(r)]$$
$$\nabla[\hat{\kappa}(r)\nabla T_1(r)] = \nabla[\hat{\alpha}(r)\hat{\sigma}(r)T_0(r)\nabla\varphi_0(r)]. \tag{22}$$

It follows from (21) that $\varphi_0(r) = 0$ owing to the boundary conditions on the potential. The system (22) makes it possible to express $\varphi_1(r)$ through the Green function:

$$\varphi_1(r) = \int_{V'} G(r, r')\nabla'_i[\sigma_{is}(r')\alpha_{sk}(r')\nabla'_k T_0(r')]\,dV'$$
$$= -\int \sigma_{is}(r')\alpha_{sk}(r')\nabla'_k T_0(r)\nabla'_i G(r, r')\,dV'. \tag{23}$$

Now we have all we need to calculate the thermocurrent:

$$\langle j_1^k\rangle = -\langle\sigma_{kl}\alpha_{lt}\nabla_t T_0\rangle + \langle\sigma_{kl}\nabla_t\varphi_1\rangle$$
$$= -\langle\sigma_{kl}\alpha_{lt}\nabla_t T_0\rangle - \int_{V'} \alpha_{sm}(r')\nabla'_m T_0(r')$$
$$\times \int_V \sigma_{is}(r')\sigma_{kl}(r)\nabla_t\nabla'_i G(r, r')\,dV\,dV'. \tag{24}$$

The inner integral can be calculated from equation (12), which gives us two components; one of them will be reduced with the first line term of the formula, while the other will take the form

$$\langle j_1^k\rangle = -E^{-1}\int_V \alpha_{sm}(r)\nabla_m T_0(r) j_{0,s}^k(r)\,dV. \tag{25}$$

The Seebeck coefficient can be easily expressed through the thermocurrent:

$$\alpha^{\text{eff}}(p) = \frac{\int_V \hat{\alpha}(r)[j_0^k(r)\cdot\nabla T_0(r)]\,dV}{\sigma_k^{\text{eff}}(p)(T_1 - T_2)EL^2}. \tag{26}$$

With the help of the Heaviside function we find

$$\alpha(r) = \alpha_1\theta_1(r) + \alpha_2\theta_2(r)$$

for the two-component medium, where $\theta_1(r)$ is 1 for the first component and 0 for the second, and $\theta_2(r) = 1 - \theta_1(r)$. After transforming the three-dimensional integral into a surface integral we obtain

$$\alpha^{\text{eff}}(p) = \int_S \alpha(r)(j_0^k(r)\cdot n)T_0(r)\,dS/[\sigma_k^{\text{eff}}(p)(T_1 - T_2)EL^2] \tag{27}$$

where n is the normal to the component interface S.

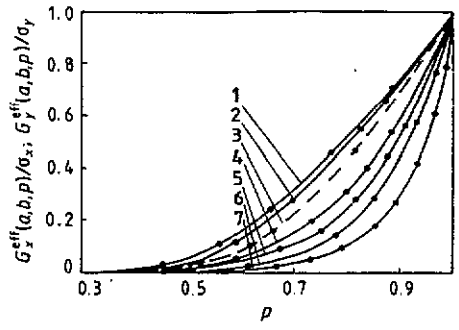

Figure 1. Effective electric conductivity versus concentration at $\sigma_z = 0.01$, $G_i^{\text{eff}}(a, b, p)$, $i = x, y$: curve 1, $G_x^{\text{eff}}(1, 100, p)$; curve 2, $G_x^{\text{eff}}(1, 5, p)$; curve 3, $G_x^{\text{eff}}(1, 1, p)$; curve 4, $G_y^{\text{eff}}(1, 5, p)$; curve 5, $G_y^{\text{eff}}(1, 15, p)$; curve 6, $G_y^{\text{eff}}(1, 50, p)$; curve 7, $G_y^{\text{eff}}(1, 100, p)$.

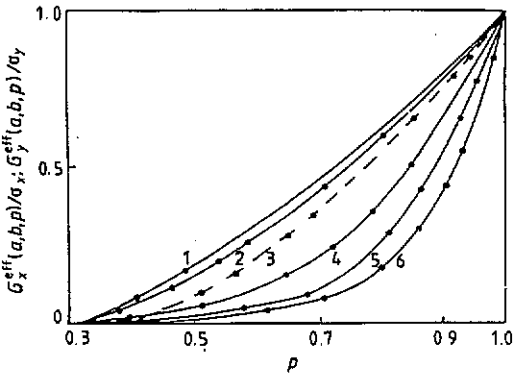

Figure 2. Effective electric conductivity versus concentration at $\sigma_z = 1$, $G_i^{\text{eff}}(a, b, p)$, $i = x, y$: curve 1, $G_x^{\text{eff}}(0.01, 1, p)$; curve 2, $G_x^{\text{eff}}(0.5, 5, p)$; curve 3, $G_x^{\text{eff}}(1, 1, p)$; curve 4, $G_y^{\text{eff}}(0.5, 5, p)$; curve 5, $G_y^{\text{eff}}(0.1, 10, p)$; curve 6, $G_y^{\text{eff}}(0.5, 50, p)$.

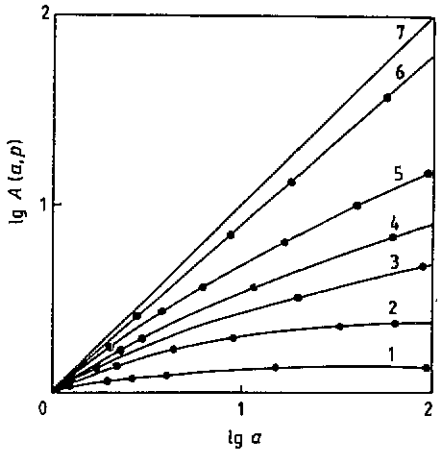

Figure 3. Functions $A(a, p)$ at $b = 0.01$ versus a at various p concentrations: curve 1, 0.45; curve 2, 0.5; curve 3, 0.6; curve 4, 0.7; curve 5, 0.8; curve 6, 0.95.

4. Conductivity

The effective anisotropic conductivity was computed for a simple cubic lattice whose bonds are provided by a random mixture of component 1 that has the tensor of electric conductivity (1) preset with probability p, and component 2 whose σ_2 has the probability $1 - p$. The system of Kirchhoff equations was solved by iteration, with the results shown in figures 1–3. Figure 1 corresponds to the quasi-two-dimensional flow of the current $\sigma_z = 0.01$ and figure 2 to the three-dimensional flow of the current $\sigma_z = 1$; the electric field is directed along the axis z. The broken curves shown on figures 1 and 2 (curves $\sigma_i^{\text{eff}}(a, p)$ where $i = x, y$) divide the families into the lower parts with anisotropy parameters exceeding unity and the upper portions with the parameter less than unity.

The biaxial anisotropy combines both extreme trends $a \to \infty$ and $a \to 0$ of the uniaxial anisotropy. This explains the introduction (Skal 1987) of a new puncture threshold p_p, which unlike other thresholds is not universal and occurs in finite samples only, its value approaching 1 with larger volume of the samples. This threshold is characterized by the

concentration when the first continuous conductive component filament emerges for the first time, connecting the opposite edges of the sample. Figure 3 shows a family of curves for different concentrations p; as p increases a number of curves

$$A(a, b, p) = \sigma_x^{\text{eff}}(a, b, p)/\sigma_y^{\text{eff}}(a, b, p)$$

are shown which are divided by the puncture threshold into those with a plateau and those going up unboundedly. The curves 1–5 on figure 3 reach a limiting plateau for sufficiently large a. The larger the p, the larger is the value of the curve reached at the plateau. For infinite samples all the curves come to a plateau because at $p \sim 1$ there always occurs a finite cluster of non-conducting component against which the continuous conductive component filament inevitably thrusts. The current flowing along this line must bypass this cluster to meet the other component, which will assure the attainment of the plateau. Over the concentration interval the conductivity 'sees' two thresholds, viz. p_{3c} and p_{2c} at $a \to 0$ or p_{3c} and p_p at $a \to \infty$ (the subscripts denote the dimensionality). With the biaxial anisotropy all three thresholds participate at the same time, i.e. the quasi-three-, two- and one-dimensional ones over the intervals $p_{3c} < p < p_{2c}$, $p_{2c} < p < p_p$ and $p > p_p$, respectively.

In order to study the critical behaviour of the kinetic coefficients, it is necessary to find limit curves (Skal 1987) that do not depend on the parameters of the anisotropy. Indices can be calculated only on such curves because the limit transition $\lim A(a, b, p) = f(p)$, with $a \to 0$, $b \to \infty$, occurs at finite parameters, which are smaller the closer they are to the threshold. In order to understand what new indices exist in the biaxial anisotropy $a \to \infty$, $b \to \infty$ and $a \to 0$, $b \to 0$ are up to a constant coincident with the uniaxial anisotropy curves $a \to 0$ and $a \to \infty$. Therefore there remains a single new case of $a \to 0$, $b \to \infty$ to which corresponds the critical index

$$\lim_{a \to 0, b \to \infty} A(a, b, p) = f(p) = 1 + \text{const}(p - p_c)^{\lambda_2} \tag{28}$$

where $\lambda_2 = 0.3 \pm 0.05$.

The effective-medium theory is known to be valid (Bernasconi 1974) in the anisotropic and isotropic cases away from the critical interval. However, unlike unsophisticated formulae for an isotropic medium, transcendental equations are involved in calculation of the anisotropic conductivity of each concentration point, and it is only when the linear approximation is applicable that explicit formulae can be obtained for the strong anisotropy limit. The formulae permit a conclusion on the existence of plateaux, which can be seen in figure 3, but the quantitative comparison of numerical data with the formulae is hindered by the fact that the theory describes infinite samples only.

The finite samples can also be described by simple equations similar to those obtained for uniaxial anisotropy (Skal 1987). Let us consider a cubic lattice each edge of which comprises nodes. The probability of the line with only component 1 nodes along the anisotropic axis $b \to \infty$ is p^N. Because the problem in question is planar, the number of such lines is Np^N, and when this value becomes equal to unity, the puncture threshold is attained, thereby validating the formula ($Np_p = 1$; $p_p = N^{-N}$)

$$\lim_{a \to 0, b \to \infty} \sigma_y^{\text{eff}}(a, b, p) = \sigma_y \exp[-N(1 - p)] \qquad 1 - p \ll 1 \tag{29}$$

which describes the deviation from the plateau and shows it to be smaller the closer it is to the concentration threshold.

5. Computed simulation of the Hall effect

The difficulties in interpretation of experimental data on the Hall effect on composite materials stem from the fact that the effect 'sees' the dimensionality of the space. Let us dwell on this in some detail. The three-dimensional space in the isotropic case is described by (Skal 1981a) $(R^{\text{eff}}(p))^{-1} \sim R_1 P(p)$. Away from the threshold the Hall coefficient should be proportional to the inverse of percolation probability while near it the curves have critical indices $g = 0.6$ and $\beta = 0.3$ respectively. This relationship naturally reflects the physical meaning of the phenomenon, i.e. the inverse value of the Hall coefficient provides information on the number of current carriers, which corresponds in the problem under discussion to the bound part of component 1 $P(p)$. The difference in the critical indices is related precisely to the fact that the Hall effect does not involve its 'dead ends' which belong to the bound compound, i.e. to $P(p)$; and because the volume responsible for the Hall effect is diminished, the critical exponent increases $g > \beta$. The disappearance of 'dead ends' away from the threshold makes the curves similar and proportional.

The same effect apparently has to happen in the two-dimensional space but it does not, which represents a peculiar feature of the phenomenon. While the conductivity and the Seebeck coefficient change little, the threshold moves from $p_{3c} = 0.33$ in the simple cubic lattice to $p_{2c} = 0.59$ in the square one, causing a shift of the curves that pass through it. The critical indices change insignificantly, for example, as regards the electric conductivity, $t_3 = 1.6$ and $t_2 = 1.1$.

Similar to the quantum Hall effect, the two-dimensional space shows a step at p_c

$$R^{\text{eff}}(p, H) = \begin{cases} R_1 & p > p_c \\ R_2 & p < p_c \end{cases} \tag{30}$$

where R_1 and R_2 are the local Hall coefficients for the components 1 and 2 respectively.

Thus when the Hall coefficient no longer provides information on the share of the volume of the conducting medium it becomes indicative of the dimensionality. A smooth transition between these extremes can be observed in thin composite films when, depending on the film thickness, the experimental data can range from $P(p)$ to a constant, which makes the data so difficult to interpret.

The critical behaviour of the Hall effect can be described by the same equation (28) as used for conductivity. It is only natural to ask here how many independent indices appear in this case. It appears that by directing the magnetic field along each coordinate axis one can obtain three limiting curves. Depending on the field direction about the anisotropy axes, the Hall coefficient demonstrates a quasi-two-dimensional pattern $H \perp a$ and a quasi-three-dimensional behaviour in the plane $H \parallel a$ and $H \perp (a, b)$ perpendicular to a plane (a, b). Both three-dimensional cases have an identical limiting curve because the ratios of the component conductivities in the planes that are perpendicular to the field are identical. Thus there exist only two independent situations shown in figures 4 and 5, to which the new critical index is related:

$$\lim_{a \to 0, b \to \infty} \frac{R^{\text{eff}}_{H \perp a}(a, b, p)}{R^{\text{eff}}_{H \parallel a}(a, b, p)} = 1 + \text{const}(p - p_c)^k \tag{31}$$

where $k = 0.15 \pm 0.05$.

Figure 4 demonstrates a smooth transition from the quasi-two-dimensional behaviour (curve 1: $a = 0.01$, $b = 1$) with a levelling out after the two-dimensional threshold,

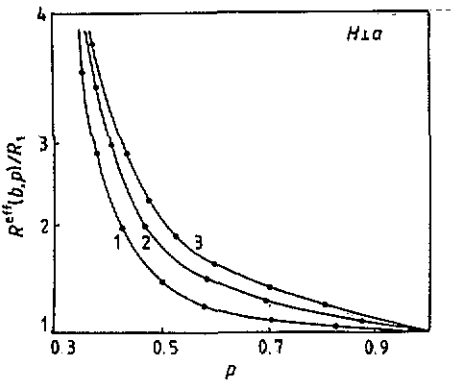

Figure 4. Effective Hall coefficient $R^{eff}_{H\perp G}(b,p)$ versus concentration at $a = 0.01$ and at various values of b: curve 1, 1; curve 2, 5; curve 3, 25.

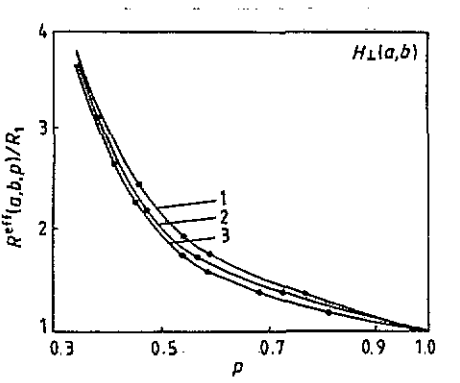

Figure 5. Effective Hall coefficient $R^{eff}_{H\parallel}(a,b,p)$ at $\sigma_z = 1$ and at various values of a and b ($H_\perp$ to plane (a,b)): curve 1, $a = b = 1$; curve 2, $a = 0.5$, $b = 5$; curve 3, $a = 0.15$, $b = 10$.

to the behaviour under conditions of a heavy magnetic field when the conductivity grows along the axis b, while the Hall coefficient tends to the three-dimensional value but never exceeds it. The reverse takes place in figure 5 where curve 1 corresponds to the isotropic case $a = b = 1$ while the growth of the anisotropic parameters $a \to 0$, $b \to \infty$ results in a downward trend of the curves.

6. Computed simulations of thermopower

While the special feature of the Hall effect is its dependence on dimensionality, the essential point for thermopower studies is the selection of an appropriate model. Both the electric conductivity and the Hall effect can be investigated on a metal–insulator model, which gives a trivial solution for the thermopower. Although this result does bring to mind the two-dimensional Hall effect, there is a difference in that in the Hall effect the total longitudinal and transverse current intersect, while in thermopower the current flows in component 1 only, component 2 making no contribution to the generation of the thermopower. The same transpires from equation (27), which shows the value of the current density projection on the normal to the component interface to be identically zero at $\sigma_2 = 0$. Therefore it is necessary to find a model representing the conductivity in the two components, which was not taken into account by Troades and Bideau (1983). In Skal (1987) it was shown that when the ratio of the thermal conductivities of the components is close to 1, the critical exponents of the electric conductivity and the thermopower are equal, but when this ratio grows, the thermopower develops a new index whose pattern is characteristic of the anisotropic percolation: the indices coincide in the first extreme case and differ in the second one.

The influence of the anisotropy on the effective Seebeck coefficient and on the electric conductivity in the two-component system can be seen from figures 6 and 7 showing these kinetic coefficients for identical local parameters. One common regularity must be emphasized: correlation of the resistance and Seebeck coefficient permits the conclusion that the thermal conductivities of the components are close, while no

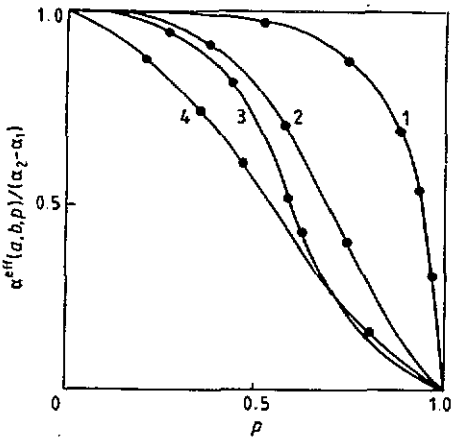

Figure 6. Effective Seebeck coefficient $\alpha^{eff}(a, b, p)$ versus concentration at $\sigma_2 = 0.01$ and at various values of a and b: $\alpha^{eff}(a, b, p)$, $a = \sigma_x/\sigma_y$, $b = \kappa_x/\kappa_y$, $\sigma_z = 0.01$; curve 1, $a = 0.014$, $b = 100$; curve 2, $a = 0.033$, $b = 0.666$; curve 3, $a = 0.25$, $b = 0.0666$; curve 4, $a = 0.8$, $b = 0.05$.

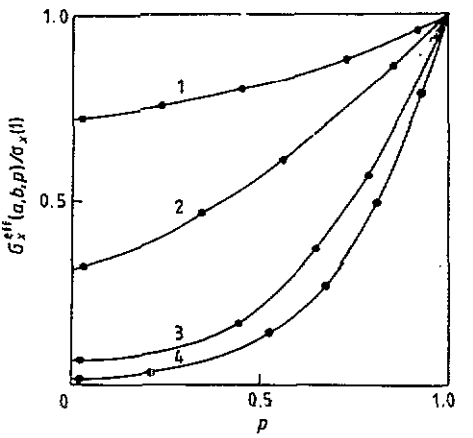

Figure 7. Effective electric conductivity $G^{eff}(a, p)$ with the same a parameters as in figure 6.

correlation is evidence of a wide gap in this parameter. This can also be seen from the accurate formula for the isotropic thermopower whose analogue for the Hall effect is

$$\alpha^{eff}(p) = (\alpha_2 - \alpha_1)\frac{\kappa^{eff}(p)/\sigma^{eff}(p) - \kappa_1/\sigma_1}{\kappa_2/\sigma_2 - \kappa_1/\sigma_1} + \alpha_1. \tag{32}$$

This equation is valid in biaxial anisotropy for the particular case of equal ratios of the electric and thermal conductivities of the components.

The critical behaviour of the thermopower can be described by

$$\lim_{a\to 0, b\to\infty} \alpha_x^{eff}(a, b, p)/\alpha_y^{eff}(a, b, p) = 1 + \text{const}(p - p_c)^m \tag{33}$$

where $m = 0.3 \pm 0.05$ when the ratio of the thermal conductivities of the component is small; otherwise the index can be expected to be different.

The critical behaviour of the Hall effect is associated only with large ratios of the components' electric conductivities $\sigma_1/\sigma_2 \to \infty$ and does not depend on local Hall coefficients. The essential point for the thermopower is that the σ_1/σ_2 or the σ_1/σ_2 and κ_1/κ_2 ratios tend to infinity, but the critical behaviour of the thermopower does not depend on local Seebeck coefficients of either component.

7. Infinite cluster model

A matter of great interest is how the infinite cluster model changes in biaxial anisotropy. At present there exist a number of such models including the one-dimensional chain (Skal and Shklovskii 1974, De Gennes 1976), fractal (Kirkpatrick 1977), drop (Coniglio 1981) and some others. The fractal and drop models have proved to be useful in renormalization group calculations. But in order to answer the questions of what a

disordered system actually looks like, if there is any regularity in this chaos, what happens in the critical interval over the concentrational axis, and what phenomena take rise in transition, use should be made of the model of 'special' points (Skal *et al* 1982, Skal 1987). The answer is that although the infinite cluster has an infinite number of properties and is seen differently by each of its kinetic coefficients, its common feature (Skal 1982) is the superlattice each side of whose cell is proportional to the correlation radius of the infinite cluster. All the reported models refer to the metal–dielectric phase transition at $p > p_c$ when an infinite cluster has already been formed and became a parameter of the transition order, but there is not a single model for the metal–superconductor transition at $p < p_c$ that would permit the determination of the order parameter of this transition. However, it is possible to develop a unified cluster model that can help us to find a unified order parameter for the two transitions, understand their similarities and differences, and clarify the phenomena occurring in the transition. Each kinetic coefficient sees the transition in its own way whether a superlattice is there or not, but it can be asserted that when there are 'special points' a superlattice exists and it does not exist when the special points are absent. In terms of the electric conductivity the infinite cluster consists of two parts, viz. the 'hot points' spaced at the correlation radius apart and concentrating all the resistance, and the superlattice formed by component 1 physically and by the ideal metal in the model. Now the question is what superlattice can take place if the infinite cluster has not come into existence at $p < p_c$. The critical interval is very small, and when the concentration approaches it from the $p < p_c$ side, the infinite cluster can be said to have taken shape. Further concentration of the critical interval changes the cluster's capacity slightly, affecting only the 'hot points', whose share is also vanishingly small, but it is precisely the 'hot points' that make the difference between the pre-threshold and post-threshold transitions, which is that the points are made up by component 2 at $p < p_c$ and by component 1 at $p > p_c$. Thus a new two-component cluster for the metal–superconductor transition is obtained, which becomes its order parameter. Hence the difference in clusters makes the transition different.

Because there have not yet been any references in the literature to a two-component cluster it is necessary to dwell on its definition. 'Hot points' are not all thin interlayers of component 2 between large clusters of component 1, but only those where a large amount of Joule heat is released; their number decreases as the threshold is approached, because component 1 is substituted for component 2, the 'hot points' get cold, and finally at the threshold there is only one last 'hot point' of component 2 which becomes the first 'hot point' of component 1, resulting in the formation of a one-component infinite cluster. Thus a two-component cluster is constructed by the electric conductivity; 'hot points' are arranged at approximately the same locations before and after the threshold. It is unimportant whether these points are located at the bonds or at the superlattice nodes; one alternative can be considered the other's dual.

How does the transition take place for other transport coefficients? The superlattice remains the same for the thermopower, with only the name of the points changed to thermopower 'active points'. These exist at high thermal conductivity ratios, disappearing at low ones and then making the notion of superlattice inapplicable.

In terms of Hall effect, 'active points' of the Hall EMF arise in geometrically different locations, these points being responsible for generation of nearly all the Hall effect. In order to unify the superlattice for three transport coefficients, we should place the 'active' Hall EMF points at its nodes and the 'hot electric conductivity points' at its bonds.

What is the effect of the anisotropy on the superlattice? In uniaxial anisotropy (Skal 1987) the superlattice is compressed along the $a \rightarrow 0$ axis and expanded along the $a \rightarrow \infty$

axis; biaxial anisotropy causes a simultaneous action of these processes, which results in concentration of 'hot points' along the $a \to 0$ axis and a reduction of their number per unit length along the axis $b \to \infty$.

To conclude, it should be stressed that for high-temperature superconductivity it is essential to determine whether the conductivity in the transition occurs over a plane or along filaments in three-dimensions. This can be calculated through use of the values of critical indices of transport coefficients and due to universality at phase transitions.

References

Bernasconi D J 1974 *Phys. Rev.* B **9** 4575

Coniglio A 981 *Disordered Systems and Localization (Lectures Notes in Physics)* ed C Castelliani and C Di Castro

De Gennes P 1976 *J. Physique Lett.* **7** L1

Kirkpatrick S 1977 *AIP Conf. Proc.* **40** 99

Last S J and Thouless D J 1971 *Phys. Rev. Lett.* **27** 1719

Lobb C D, Frank D J and Tinkman M 1981 *Phys. Rev.* B **2** 2262

Sarychev A K and Vinogradov A P 1983 *J. Phys. C: Solid State Phys.* **16** L1073

Shklovskii B I 1978 *Phys. Status Solidi* b **75** K111

Skal A S 1981a *Sov. Phys.–Dokl.* **260** 602

—— 1981b *J. Techn. Phys.* **11** 2443

—— 1982 *Phil. Mag.* B **45** 335

—— 1985 *J. Phys. C: Solid State Phys.* **18** 3483

—— 1987 *J. Phys. C: Solid State Phys.* **20** 245

Skal A S, Andreev A A and Tschirner N U 1982 *Phil. Mag.* **45** 323

Skal A S and Shklovskii B I 1974 *J. Phys. Semicond.* **8** 1586

Straley J P 1980 *J. Phys. C: Solid State Phys.* **13** L773

Troades J P and Bideau D 1983 *J. Phys. C: Solid State Phys.* **16** 1069

Vannimenus J and Knezevic M J 1984 *J. Phys. C: Solid State Phys.* **17** 4927